

# A variation on the Chamberlin trimetric map projection

## ARTICLE HISTORY

Compiled June 30, 2021

## ABSTRACT

We present a variation on the Chamberlin trimetric map projection. This new projection, which we call the matrix trimetric projection, consists of a linear transformation of the squares of the distances between a given point and three control points. The formula of the forward projection is simpler than the Chamberlin projection, and admits an inverse formula which requires numerical iteration of only one parameter. We make comparisons between the two projections using a representative list of control points. The Chamberlin trimetric projection outperforms the matrix trimetric projection on measures of angle deformation and scale deformation, but the opposite is true for a measure of distance deformation, and the difference between the results of the projections is small over all measures. The forward Matrix trimetric projection can be calculated in half the time of the Chamberlin trimetric projection. We conclude that the matrix trimetric projection is a viable alternative to the Chamberlin trimetric projection, especially if an inverse is required or speed is important.

*Keywords:* Chamberlin trimetric, matrix trimetric, projection, cartography, distortion, distance, triangulation

## 1. Introduction

Any map projection must introduce some form of distortion. In particular, no map projection can be both conformal (angle-preserving) and equal-area. Projections that eliminate one form of distortion often introduce a great deal of another form of distortion. For example, many conformal projections drastically enlarge some areas compared to others, most notoriously the Mercator projection, but also the stereographic and the Lambert conformal conic projections. (Snyder, 1987) A compromise map projection is one that seeks to balance different kinds of distortion: allowing some amount of different kinds of distortion can produce a map where none of the distortion is conspicuous.

The Chamberlin trimetric projection (CTP) is such a compromise map projection. It is named for Wellman Chamberlin, a chief cartographer for the National Geographic Society, which has published wall and atlas maps using his projection. (Christensen, 1992) The CTP is appropriate for mapping whole continents and large portions of continents. It may be thought of as a form of triangulation. It can also be considered part of an “ $n$ -metric” family of projections with the azimuthal equidistant projection and the two-point equidistant projection, which depend on measurements from a single point and pair of points, respectively. (Snyder, 1987) Being a compromise projection, the CTP does not perfectly preserve angle, area, or distance. Most often, the CTP is used with the spherical approximation of the Earth: for practical ellipsoids, distortions due to the spherical approximation are negligible compared to distortions due to the projection itself.

The CTP is based on a simple geometric construction, using three arbitrary control points on the sphere. However, modern computerized GISes require algebraic formulas, which are somewhat involved for the CTP. These formulas are presented in Christensen (1992), and can be seen in the source code to its implementation in PROJ contributors (2019). In general, the length of the algorithm relates to its speed of execution. In particular, the algorithmic form has branching logic depending on where the given point lies with respect to the geodesics between control points, which (as Christensen (1992) observed) can cause numerical issues.

We present a new map projection called the matrix trimetric projection (MTP) as an alternative to the CTP. A geometric construction related to the CTP results in a map projection that is similar but has a simpler formula. This formula is a closed-form matrix function of the squares of the distances, and allows for a tractable inverse. As the derivations involve matrices and linear algebra, refer to a text such as Strang (1980) if needed.

## 2. Preliminaries

These projections will almost always be implemented using the spherical approximation. Formulas for that approximation are given shortly, and we’ll refer to “the sphere” instead of “the ellipsoid”. In fact, the forward formulas for the CTP and MTP are agnostic of the surface to be projected, depending only on the result of the distance function.

We denote points on the sphere by  $\mathbf{v}$  or subscripted versions.  $\mathbf{v}$  is a 3-vector with unit length lying on the unit sphere. Using this vector form allows us to take advantage of linear algebra. Points specified by latitude  $\varphi$  and longitude  $\lambda$  can be converted to a unit vector as so: (Lapaine, 2017)

$$\mathbf{v} = \begin{bmatrix} x \\ y \\ z \end{bmatrix} = \begin{bmatrix} \cos(\varphi) \cos(\lambda) \\ \cos(\varphi) \sin(\lambda) \\ \sin(\varphi) \end{bmatrix}. \quad (1)$$

The reverse conversion is:

$$\begin{aligned} \varphi &= \arctan \left( \frac{z}{\sqrt{y^2 + x^2}} \right), \\ \lambda &= \arctan(y, x), \end{aligned} \quad (2)$$

where the 2-variable form of  $\arctan$ , commonly called `arctan2` or `atan2` in numeric software libraries, is used for  $\lambda$ .

One statement of the distance function on the sphere is

$$d(\mathbf{v}_i, \mathbf{v}_j) = R \arccos(\mathbf{v}_i \cdot \mathbf{v}_j) \quad (3)$$

where  $R$  is the radius of the sphere. We use a radius of 6,371 km, approximately equal to the most common mean radii of the Earth. (Snyder, 1987) There are equivalent functions in terms of vectors that are more numerically stable for certain range of arguments, but this is the form we will use for derivations.

We denote points in the Euclidean plane by  $\mathbf{p} = [x, y]$  and subscripted versions. Planar distances are found using the usual Euclidean norm:  $\|\mathbf{p}_a - \mathbf{p}_b\|$ .

Let  $\mathbf{v}_1, \mathbf{v}_2, \mathbf{v}_3$  be control points on the sphere, in counter-clockwise order, and let  $\mathbf{V}$  be the matrix having  $\mathbf{v}_i$  as its  $i$ th column. Let  $\mathbf{p}_1$  etc. be the control points on the plane, in corresponding order, and  $\mathbf{P}$  be the matrix having  $\mathbf{p}_i$  as its  $i$ th column. The triangles with vertices at  $\mathbf{v}_i$  or  $\mathbf{p}_i$  are called the control triangles: spherical or planar control triangle, respectively, if the distinction is important. The control points are usually chosen so that the control triangle contains or mostly contains the geographic region of interest. For this paper, very small triangles are excluded, as are triangles with areas of an entire hemisphere or more: neither are typical use cases for the CTP. Note that the planar control triangle is **not** the image of the spherical control triangle under either projection! That image is slightly larger, containing the planar control triangle, and has curved edges.

For both projections,  $\mathbf{p}_i$  must be arranged such that  $d(\mathbf{v}_i, \mathbf{v}_j) = \|\mathbf{p}_i - \mathbf{p}_j\|$  for all  $i$  and  $j$  in  $\{1, 2, 3\}$ : the spherical length of the edges of the spherical control triangle are equal to the Euclidean lengths of the planar control triangles. Without loss of generality, also assume that  $\|\mathbf{p}_i\|$  is the same for all  $i$ , such that the circumcenter of the control triangle lies at the origin. This assumption just removes a translation in the plane in order to simplify the formula for the MTP: false northing and easting can be added later. Given  $\mathbf{v}_i$ ,  $\mathbf{p}_i$  can be constructed as follows. Let  $i, j, k$  be a cyclic permutation of  $\{1, 2, 3\}$ , and let  $s_k = d(\mathbf{v}_i, \mathbf{v}_j)$ , such that side  $k$  with length  $s_k$  is opposite point  $k$ . The circumradius of the Euclidean triangle with sides of length  $s_k$  is (Isaacs, 2009)

$$C = \frac{\prod_i s_i}{\sqrt{\sum_i 2s_i^2 s_j^2 - s_i^4}}. \quad (4)$$

From the (Euclidean) law of cosines, the interior angle  $\phi_i$  at each vertex is

$$\phi_i = \arccos\left(\frac{s_k^2 + s_j^2 - s_i^2}{2s_k s_j}\right). \quad (5)$$

Then a set of points satisfying the requirements are given as so:

$$\mathbf{P} = \begin{bmatrix} C \cos(2\phi_2) & C \cos(2\phi_1) & C \\ C \sin(2\phi_2) & -C \sin(2\phi_1) & 0 \end{bmatrix}. \quad (6)$$

These points can be rotated about the origin as desired. Note that some intermediate values in Equation 4 may be large. This should not cause a problem on modern computers using common geographic units of distance, but one may wish to use a unit of measurement such as radians of arc in these calculations and then scale the result accordingly.

### 3. Forward projection

Figure 1 shows the geometric construction of the CTP and MTP. We start with the CTP. Let  $\mathbf{v}$  denote the point to project, and let  $r_i = d(\mathbf{v}_i, \mathbf{v})$  be the true distances from each control point to  $\mathbf{v}$ . Figure 1a shows the control triangle on the sphere

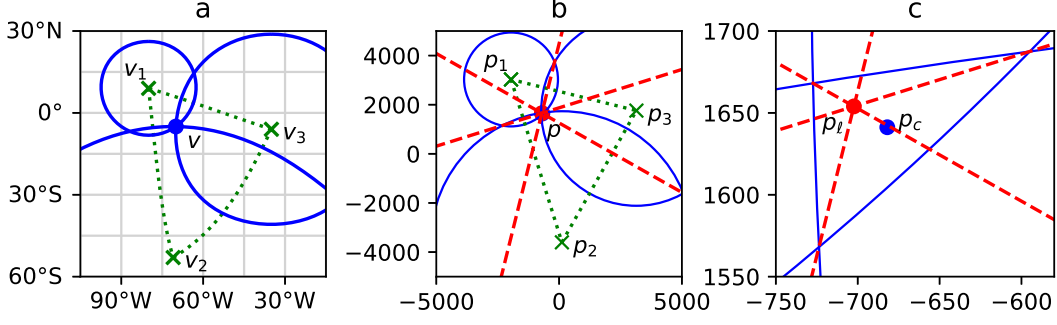


**Figure 1.** Construction of the CTP and MTP. Plot 1a is in equirectangular projection. Plot 1b is the result of the CTP or MTP in the plane. Plot 1c is the same as plot 1b, zoomed in to the small triangle created by the three circles.  $\mathbf{p}_c$  is the point projected by the CTP and  $\mathbf{p}_m$  is the point projected by the MTP. Green dotted lines indicate the control triangles, the circles are blue solid lines, and the perpendiculars are red dashes.

with vertices  $\mathbf{v}_i$ , the given point  $\mathbf{v}$ , and circles of radius  $r_i$  centered on  $\mathbf{v}_i$  and passing through  $\mathbf{v}$ . Moving to the plane, Figure 1b shows circles of the same radius  $r_i$  centered on the planar control points  $\mathbf{p}_i$ . The circles appear to all intersect at a single point, but due to the difference in curvature between the sphere and the plane they in fact form a small triangle with curved edges, as shown in Figure 1c. In the time of manual plotters the exact definition of this point was less important, but Christensen (1992) and modern implementations (e.g. PROJ contributors, 2019) use the centroid of the small triangle, denoted  $\mathbf{p}_c$ . Note that each pair of circles intersects in (at most) two points, so the algorithm must choose which point makes up the small triangle. In Christensen (1992) this is done by comparing the azimuths between each pair of control points to the azimuths from each control point to the given point.

Construction of the MTP starts like the CTP. If one draws a line through the two points of intersection of each pair of circles, that line is perpendicular to the triangle edge. These are the dashed red lines in Figure 1b and c. The three lines, one for each pair of circles, appear to meet at a single point: this observation can be proven with a simple triangle theorem sometimes attributed to Carnot. (Posamentier & Salkind, 1996; Wohlgemuth, 2010) That point of intersection is denoted  $\mathbf{p}_m$ . For most points within the control triangle  $\mathbf{p}_m$  lies within the small triangle, although this is not true in general and is not necessary to create a valid map projection. (If  $\mathbf{v}$  lies on a control triangle edge, one pair of circles has a single point of intersection. In that case, draw a perpendicular to the control triangle edge through that point of intersection and continue as in the general case.)

The equations of each perpendicular line, taken together, create a linear system. It is an overdetermined system of 3 equations in 2 variables, but since all 3 lines meet at the same point, it has a solution. Ultimately this system can be solved for  $\mathbf{p}_m$  to define a forward map projection as follows.

$$\mathbf{p}_m = \mathbf{M} \begin{bmatrix} r_1^2 & r_2^2 & r_3^2 \end{bmatrix}^\top, \quad (7)$$

$$\mathbf{M} = \frac{1}{2T} \begin{bmatrix} y_3 - y_2 & y_1 - y_3 & y_2 - y_1 \\ x_2 - x_3 & x_3 - x_1 & x_1 - x_2 \end{bmatrix} = \frac{1}{2T} \begin{bmatrix} 0 & -1 \\ 1 & 0 \end{bmatrix} \mathbf{P} \begin{bmatrix} 0 & -1 & 1 \\ 1 & 0 & -1 \\ -1 & 1 & 0 \end{bmatrix}, \quad (8)$$

$$T = \begin{vmatrix} x_1 & x_2 & x_3 \\ y_1 & y_2 & y_3 \\ 1 & 1 & 1 \end{vmatrix}. \quad (9)$$

$T$  is equal to twice the area of the Euclidean control triangle.

The matrix  $\mathbf{M}$  has a (right) nullspace spanned by the vector  $[1, 1, 1]^\top$ . This implies the MTP is not one-to-one for all possible values of  $r_i$ . For example, for any values of  $r_i$  such that  $r_1 = r_2 = r_3$ , then  $\mathbf{p}_m = [0, 0]^\top$ . Like the CTP, the MTP projects the entire sphere to a bounded portion of the plane: the boundary of that portion can be termed the boundary of the projection. There is a region of overlap that is mapped into the same area but in reverse orientation. That region includes the antipodes of the control points. In real applications, the overlap region of the sphere is not of interest and can be excluded.

#### 4. Inverse projection

Given  $\mathbf{p}_m$ , start to invert the projection as so:

$$[k_1 \quad k_2 \quad k_3]^\top = \mathbf{M}^+ \mathbf{p}_m, \quad (10)$$

$$\mathbf{M}^+ = \frac{2}{3} \begin{bmatrix} -2x_1 + x_2 + x_3 & -2y_1 + y_2 + y_3 \\ x_1 - 2x_2 + x_3 & y_1 - 2y_2 + y_3 \\ x_1 + x_2 - 2x_3 & y_1 + y_2 - 2y_3 \end{bmatrix} = \frac{2}{3} \begin{bmatrix} -2 & 1 & 1 \\ 1 & -2 & 1 \\ 1 & 1 & -2 \end{bmatrix} \mathbf{P}^\top. \quad (11)$$

$k_i = r_i^2 - h$  for some value of the free parameter  $h$ . This is a general solution to inverting Equation 7:  $\mathbf{M}^+$  is the pseudoinverse of  $\mathbf{M}$  and vice versa. Because  $\mathbf{M}^+$  has a left nullspace spanned by the vector  $[1, 1, 1]$ , it follows that  $\sum_i k_i = 0$ , and then that  $h = \frac{1}{3} \sum_i r_i^2$ . These equations are not enough to determine  $r_i$  and  $\mathbf{v}$ : information about the sphere needs to be introduced.

To simplify the derivation, use  $R = 1$ , such that distance on the surface of the sphere has units of radians of arc. The circle of points  $\mathbf{v}$  at distance  $r_i$  from a point  $\mathbf{v}_i$  is simply the circle created by a plane intersecting the sphere. Rearranging the distance function, this plane may be specified as  $\mathbf{v}_i \cdot \mathbf{v} = \cos(r_i)$ . These planes combined together give a linear system. Thus,

$$\mathbf{v} = \mathbf{V}^{-1} [\cos(r_1) \quad \cos(r_2) \quad \cos(r_3)]^\top. \quad (12)$$

For the point to lie on the unit sphere,  $\|\mathbf{v}\| = 1$ . Let  $\mathbf{c}$  be a vector with  $i$ th component  $\cos(r_i)$ . Then,  $\mathbf{c}^\top (\mathbf{V}^\top \mathbf{V})^{-1} \mathbf{c} = 1$ . Make the substitution

$$r_i = \sqrt{k_i + h}. \quad (13)$$

We now have an equation with one unknown,  $h$ .

Some obvious bounds can be placed on  $h$ . In units of radians,  $0 \leq r_i \leq \pi$ . Since this must hold for every  $r_i$ , it follows that

$$h_{\min} = -\min_i k_i \leq h \leq \pi^2 - \max_i k_i = h_{\max}. \quad (14)$$

Within these bounds, there may be at most two solutions for  $h$ . The solution with smaller  $h$  is the desired one, and the one with larger  $h$  corresponds to the overlap region.

Let  $\mathbf{A} = (\mathbf{V}^\top \mathbf{V})^{-1}$  and

$$f(h) = \mathbf{c}^\top \mathbf{A} \mathbf{c} - 1. \quad (15)$$

The derivative of  $f(h)$  is

$$f'(h) = -\mathbf{c}^\top \mathbf{A} \mathbf{b}, \quad (16)$$

where  $\mathbf{b}$  is a vector with  $i$ th component  $\sin(\sqrt{k_i + h})$ . Note that  $f'(h)$  and  $f(h)$  share many of the same terms, which can be exploited for more efficient calculation. Given all the preceding, Newton's method can be applied to solve for  $h$ . A suitable initial condition is  $h = h_{\min}$ , which satisfies  $f(h) = 0$  at the control points. This initial condition consistently results in convergence to the lower root of  $f(h)$ .

The error is roughly proportional to the final value of  $|f(h)|$ . A stopping condition of  $|f(h)| < 10^{-4}$  results in an accuracy of 1 meter or better. For points in or near the control triangle, this condition is met in only a few iterations. Convergence is somewhat slower farther away from the control triangle. At the boundary of the projection, the lower solution and upper solution are the same and  $f(h) = f'(h) = 0$  so Newton's method converges at a merely linear rate. (Burden & Faires, 2006)

## 5. Comparison

The open-source C++ package PROJ (PROJ contributors, 2019) contains an implementation of the CTP. We implemented the MTP as a patch to PROJ, to enable a fair comparison of computation time, and to take advantage of its existing framework.

We use a set of control triangles, recorded in Table 1, that is the same as Christensen (1992, p. 90). These serve as a set of test cases for comparing the CTP and MTP. The length of each side and the area of each triangle (with the spherical approximation given earlier) is also given, and the control triangles are sorted by area.

To measure distortion of area and angle, we use the areal scale factor  $s$  and maximum angular deformation  $\omega$  as defined in equations 12–15, 27, and 28 in section 4 of Snyder (1987). These are implemented in the `proj_factors()` function of PROJ, which estimates the derivatives numerically. For the projections in this text it makes sense to measure distance distortions with regards to the distance between a given point and the control points. Let  $r_i = d(\mathbf{v}_i, \mathbf{v})$  be the distance from  $\mathbf{v}_i$  to  $\mathbf{v}$  on the sphere, as earlier, and let  $\ell_i = \|\mathbf{p}_i - \mathbf{p}\|$  be the distance from  $\mathbf{p}_i$  to  $\mathbf{p}$  in the plane. Our new measure, the total distance deviation or  $D$ , is the sum of differences in the distances measured on projected and unprojected distances:

$$D = \sum_i |r_i - \ell_i|. \quad (17)$$

For each spherical control triangle, summary statistics for  $\omega$ ,  $D$ , and  $s$  are shown in Figures 2–4. Note that the control triangles are sorted by area in these figures as well. These statistics are measured within the spherical control triangles, and should not be taken to summarize the entire map: in most cases, the region of interest extends

Region	Point			Side length			Area
	1	2	3	1	2	3	
Africa Wall	19°3'W, 24°25'N	20°E, 35°S	59°3'E, 24°25'N	7,783	7,785	7,783	32.38
North America Wall	150°W, 55°N	92°30'W, 10°N	35°W, 55°N	7,064	6,434	7,064	23.71
South America Wall	80°W, 9°N	71°W, 53°S	35°W, 6°S	6,161	5,259	6,947	17.70
Europe Wall	15°E, 72°N	8°W, 33°N	38°E, 33°N	4,254	4,541	4,541	9.09
E South America	63°33'W, 8°8'N	58°33'W, 34°35'S	35°13'W, 5°47'S	4,000	3,502	4,779	7.25
S South America	43°W, 18°S	72°W, 18°S	72°W, 56°S	4,225	4,874	3,064	6.77
Australia	134°E, 8°S	110°E, 32°S	158°E, 32°S	4,487	3,643	3,643	6.76
NW South America	69°W, 25°S	55°W, 10°N	85°W, 10°N	3,284	4,261	4,177	6.70
Canada Wall	150°W, 60°N	97°30'W, 50°N	45°W, 60°N	3,423	5,197	3,423	6.11
Canada Atlas	98°13'W, 61°39'N	135°W, 40°N	55°W, 40°N	6,560	3,761	3,449	5.28

**Table 1.** Table of control triangles and their measurements. Coordinates are from Christensen (1992). Side  $n$  is opposite point  $n$ . Lengths are in km, and areas are in millions of square km. Measurements use spherical approximation.

outside the triangle. Rather, the statistics allow a quantitative comparison of the two projections.

As shown in Figure 2, the MTP consistently has a larger  $\omega$  than the CTP: in fact, the maximum  $\omega$  for the CTP is near the average  $\omega$  for the MTP. Maximum and average  $\omega$  trend upwards with control triangle area, although asymmetry of the control triangle has some influence too, as can be seen in the Canada triangles. The maximum  $\omega$  for the MTP is about 3 times that for the CTP, and the average  $\omega$  is about 3 to 4 times. However, for moderately-sized triangles, the maximum  $\omega$  values are small for both projections, not exceeding 6°. Even for the large triangles – Africa, North America, and South America Wall Maps – the maximum distortion is tolerable, and the average does not exceed 6°.

Total distance deviation  $D$  in Figure 3 shows an even clearer trend, monotonically increasing with triangle area. Both projections have the same maximum  $D$  values. The MTP has consistently lower average  $D$  values than the CTP: among these triangles, the maximum  $D$  for the CTP is about 1.35 to 1.4 times the maximum  $D$  for the MTP. The worst distortion, Africa Wall Map’s maximum  $D$ , is less than 5% of its edge lengths, and smaller control triangles have a maximum  $D$  that is an even smaller percent.

As true 1:1 scale maps are impractical, absolute values of  $s$  are unimportant: the quantity  $\sigma = \frac{\max s}{\min s} - 1$  is plotted in Figure 4 instead. The trend of  $\sigma$  is less clear. A combination of control triangle area and asymmetry influences this value. In general, this value is higher for MTP than CTP, but not by any consistent factor, and for the large and symmetric Africa Wall Map triangle the MTP is actually lower than the CTP. The amount of scale distortion is small for both: except for the very obtuse

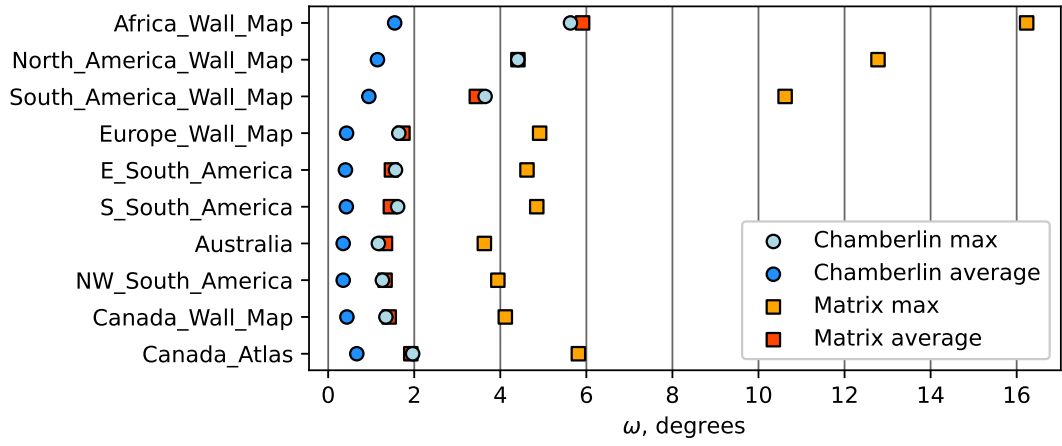


**Figure 2.** Comparison of maximum angular deformation  $\omega$ .

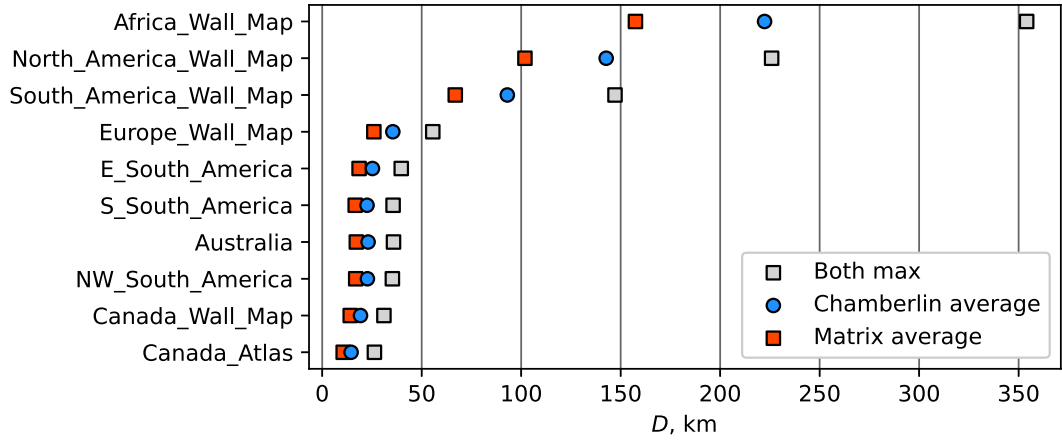


**Figure 3.** Comparison of total distance deviation  $D$ .

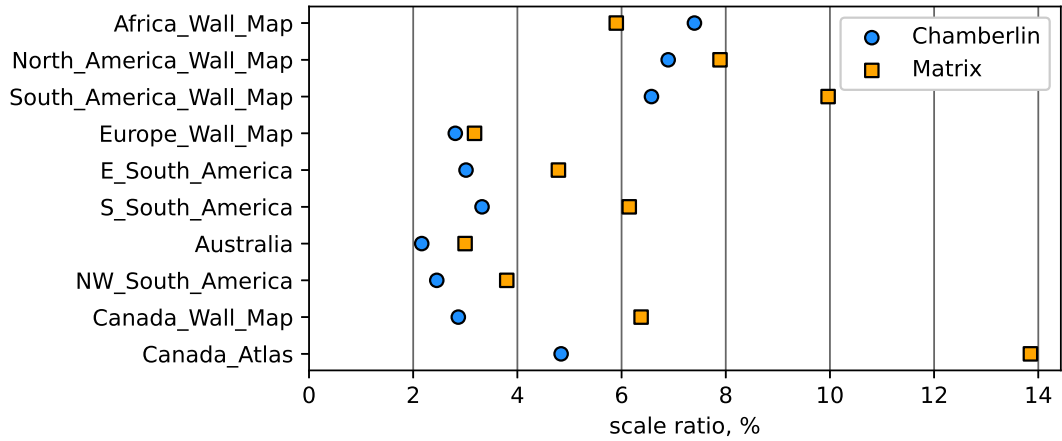


**Figure 4.** Comparison of areal scale ratio  $\sigma$ .



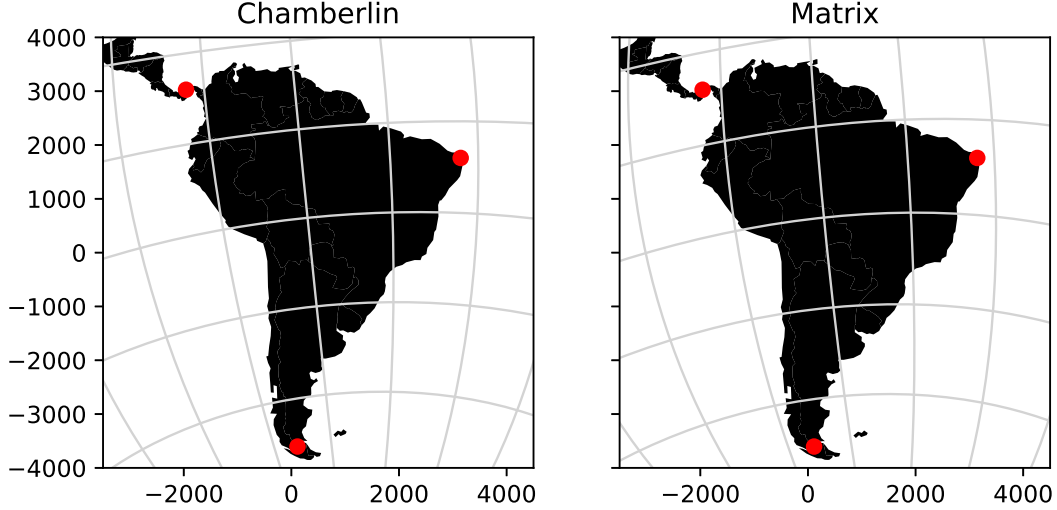


**Figure 5.** Projection of South America and surroundings. In this and the following figures, red dots indicate the control points.

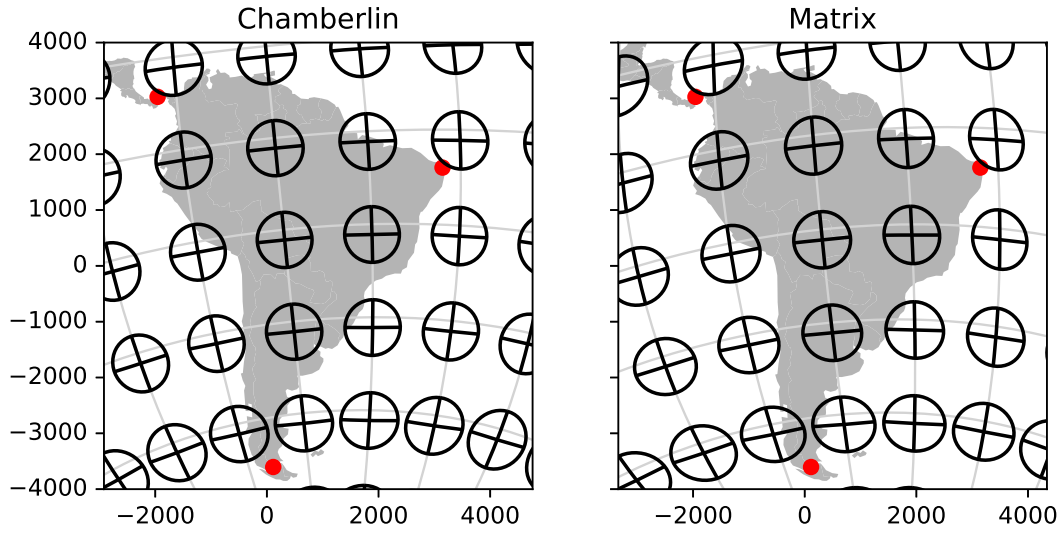
Canada Atlas triangle, all values are below 10%.

A comparison of the two projections using the South America Wall Map control points is in Figure 5. The South America Wall Map control triangle is fairly representative, being somewhat asymmetric but not too obtuse. The small part of Central America in the upper left is somewhat shifted between the two maps, as is the western area near Ecuador and Peru, but no features on either map are conspicuously distorted compared to the other. Figure 6 shows ellipses of distortion with centers on a grid at steps of  $15^\circ$  latitude and longitude. Distortion is somewhat more visible in this figure: one can see that the MTP introduces slightly more non-conformal distortion near the control points.

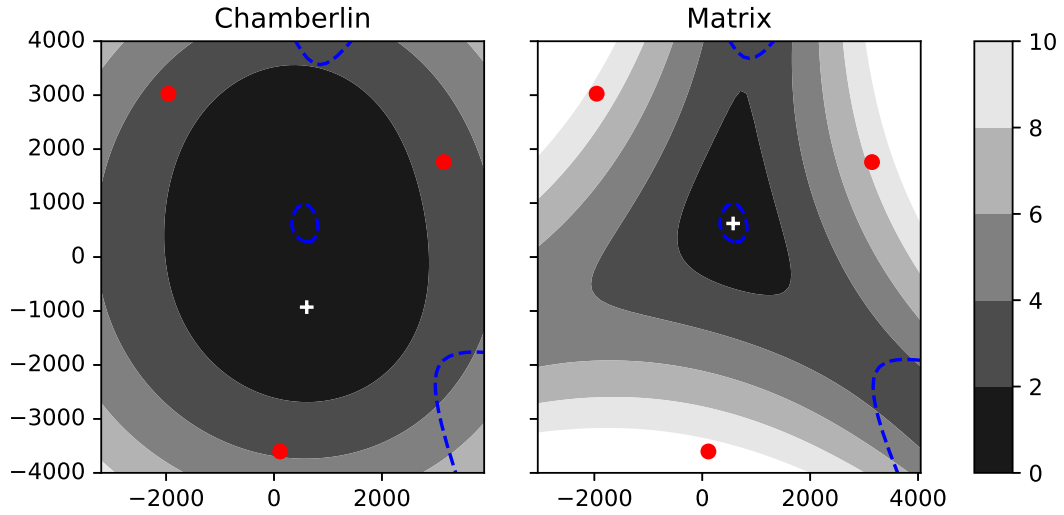
Contour lines of  $\omega$  are shown in Figure 7. Those in the CTP are ovals, while those for the MTP extend outward through each edge of the control triangle. Both reach a minimum  $\omega$  of 0 at a point inside the control triangle. Highly obtuse control triangles, like Canada Atlas, may have two local minima for  $\omega$  within the control triangle.  $\omega$  is higher for MTP than CTP, except for a small region in the control triangle where both are near 0 and some regions near the boundary of the map.

Figure 8 depicts contour lines of  $D$  for these two projections. Both projections have a local minimum of 0 at the control points, which follows from the geometric construction. Both have a local maximum inside the control triangle.  $D$  for the MTP is low along the control triangle edges, while for the CTP it is larger.  $D$  is lower for MTP than CTP in a region including the control triangle and nearly all of South America, except for a small region near the shared maximum. It is also lower along the lines extending out along the edges of the control triangle.  $D$  does increase more rapidly for the MTP than the CTP in the other regions outside the triangle as one moves away from the control triangle.

Contour lines of  $s$  are shown in Figure 9. The contour lines have the same elliptical structure in both projections, centered on a point where  $s$  reaches a local minimum. This point, and the minimum value there, is different for each projection. That influences the differences in aggregate area distortion in Figure 4. The spherical control triangle is projected to a slightly different shape for each projection, which influences



**Figure 6.** Ellipses of distortion, on a  $15^\circ$  grid.



**Figure 7.** Maximum angular deformation  $\omega$ , in degrees. Blue dashed lines indicate where the two projections have equal  $\omega$  values. The white + symbol indicates where  $\omega$  attains the minimum value of  $0^\circ$ .

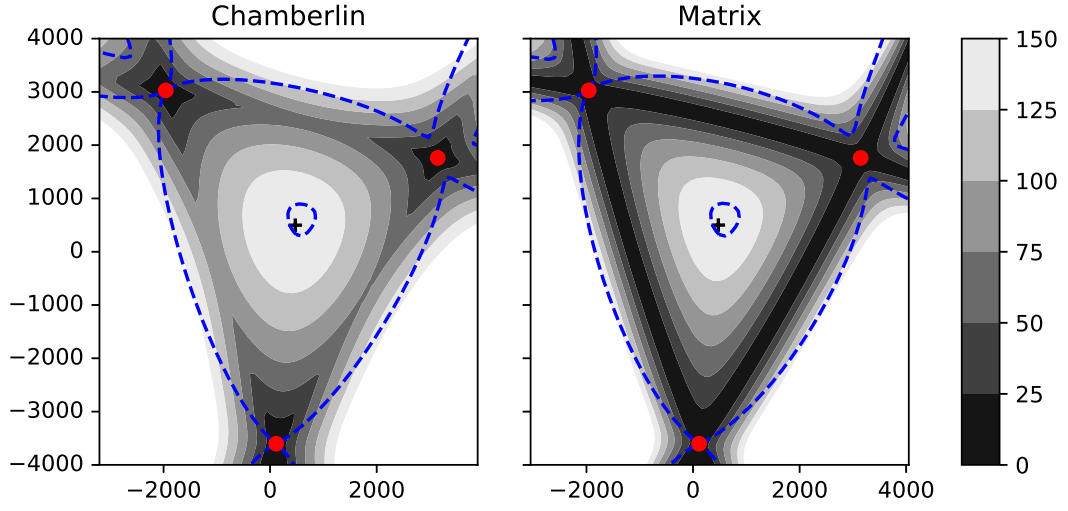


**Figure 8.** Total distance deviation  $D$ . Blue dashed lines indicate where the two projections have equal  $D$  values. The black  $+$  symbol indicates where  $D$  attains a local maximum of 147 meters.

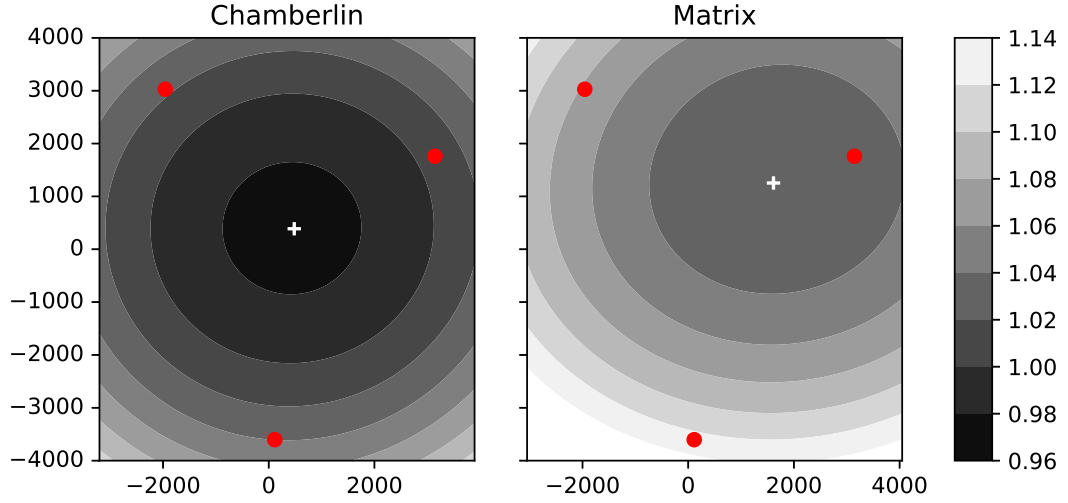


**Figure 9.** Areal scale factor  $s$ . The white  $+$  symbol indicates where  $s$  attains a local minimum: 0.974 for CTP and 1.022 for MTP.

Projection	Time (s)	Time minus overhead (s)
CTP	3.42	3.40
MTP	1.63	1.62
No-op	0.02	0.00

**Table 2.** Computation time comparison.

the unscaled values of  $s$  as well.

In most practical applications the area pictured in these figures will be sufficient, but we can state trends as both projections extend outward from the control triangle, outside the area shown in these figures.  $\omega$  increases to  $180^\circ$  at the projection boundary, and increases further in the overlap region, representing the inversion there.  $D$  generally increases away from the center, but for the MTP  $D$  remains low on the control triangle edges.  $s$  is bounded for the entire sphere: it increases to a maximum and then decreases to 0 at the projection boundary. In the overlap region,  $s$  becomes negative and reaches a minimum value.

To determine computation time, the `timeit` package in Python (Van Rossum & Drake, 2009) was used with the PyProj interface to PROJ. (Snow et al., 2020) A data set of 64,800 points across the sphere was projected 100 times. This was repeated 5 times for each control triangle, and the lowest total time of those 5 was recorded, as recommended by the `timeit` documentation. This was done for the two projections and a “no-op” projection that returns the input unchanged, used to estimate overhead. Only the transformation itself was timed, not the initialization of the projection: the initialization time is negligible compared to the time cost of running the projection repeatedly. As expected, the timing differences between control triangles were not significant for either projection. Table 2 shows the minimum runtimes across all control triangles. Accounting for overhead, the MTP takes slightly less than half the time of the CTP.

## 6. Conclusion

We have presented a new compromise map projection, the matrix trimetric projection (MTP), and demonstrated that it is a suitable alternative to the Chamberlin trimetric projection (CTP). In general, the differences between the results of the CTP and MTP are small. The MTP has the advantage if an inverse is needed, if one wishes to reduce the distance distortion described earlier, or if processing time is a concern. The CTP is useful for creating maps of continents with low levels of various types of distortion, but is uncommon in contemporary cartography: the advantages of the MTP may open it up to new uses.

The forward formula for the MTP is given in Equations 7–9. Equation 7 is a simple product of a matrix and a vector. The vector depends on the point being transformed. The matrix calculated by the latter two equations depends only on the control points, so can be calculated once and reused. Measuring points transformed per unit time, the MTP is about twice as fast as the CTP. Of course, details of the software influence the speed comparison, but PROJ’s implementation of the CTP is itself fairly short, does not have any obvious inefficiencies, and has changed little in more than two decades.

The inverse formula for the MTP is calculated by Equations 10–13 and a single-variable Newton’s method iteration using Equations 15 and 16. The matrices in Equations 11 and 12, as well as matrix  $\mathbf{A}$  in Equations 15 and 16, also depend only on the

control points and can be reused. The CTP, in contrast, has no known inverse aside from the general methods used to invert a two-variable function, which are slow and often unstable.

Figures 2–4 plot aggregate measures of distortion within each of the listed control triangles. The CTP outperforms the MTP in terms of angular distortion and (except in one case) scale distortion, but the reverse is true for distance distortion. In most cases, the differences between the two are small in absolute terms. For both projections, distortion tends to be larger for a larger control triangle. Figures 5–8 show the projections applied to South America, demonstrating the shape of distortions across the mapped area. Differences between the two projections in Figure 5 are difficult to notice visually.

The same control points were used for both projections in this work, but the optimal placement of control points may be somewhat different for the application of different projections to the same geographic feature. The angular distortion of the MTP is lower in a region extending through the middle of the control triangle edges, so one may wish to orient the triangle to take advantage of that. One may also wish to avoid the area outside the triangle where  $D$  increases more rapidly for the MTP than the CTP.

The form of the MTP’s forward formula suggests a possible family of projections that are simple functions of distances to control points, such as a polynomial function. Additionally, there may exist similar projections using measurements other than distance, such as area.

## 7. Data availability statement

A software implementation of the MTP, as well as code used to produce the calculations and figures in this text, is available at the private link <https://figshare.com/s/d2f92fa8ae678cdd382c>. On acceptance this link will be replaced with an openly accessible site, subject to Creative Commons license.

Figures in this text were created using the Python packages matplotlib (Hunter, 2007) and GeoPandas (Jordahl et al., 2020), and their dependencies including PROJ (PROJ contributors, 2019) and PyProj (Snow et al., 2020) as referenced earlier. Land mass shape data come from Patterson and Kelso (2020).

## References

- Burden, R., & Faires, J. (2006). Solutions of equations in one variable. In *Numerical analysis* (8.1 ed., pp. 67–85). Cengage Learning.
- Christensen, A. H. (1992). The chamberlin trimetric projection. *Cartography and Geographic Information Systems*, 19(2), 88-100.
- Hunter, J. D. (2007). Matplotlib: A 2d graphics environment. *Computing in Science Engineering*, 9(3), 90-95.
- Isaacs, I. (2009). Triangles. In *Geometry for college students* (pp. 50–93). American Mathematical Society.
- Jordahl, K., den Bossche, J. V., Fleischmann, M., Wasserman, J., McBride, J., Gerard, J., ... Leblanc, F. (2020). *geopandas/geopandas: v0.8.1*. <https://zenodo.org/record/3946761>. Zenodo.

- Lapaine, M. (2017). Modelling the world. In A. Kent & P. Vujakovic (Eds.), *The Routledge handbook of mapping and cartography* (pp. 187–201). Taylor & Francis.
- Patterson, T., & Kelso, N. V. (2020). *Natural earth*. <https://www.naturalearthdata.com/>. (Accessed: 2020-01-17)
- Posamentier, A., & Salkind, C. (1996). The Pythagorean theorem. In *Challenging problems in geometry* (pp. 85–86). Dover Publications.
- PROJ contributors. (2019). PROJ coordinate transformation software library [Computer software manual]. Retrieved from <https://proj.org/>
- Snow, A. D., Whitaker, J., Cochran, M., den Bossche, J. V., Mayo, C., de Kloe, J., ... Taves, M. (2020, November). *pyproj4/pyproj: 3.0.0*. Zenodo. Retrieved from <https://doi.org/10.5281/zenodo.4247339>
- Snyder, J. P. (1987). *Map projections—a working manual* (No. 1395). US Government Printing Office.
- Strang, G. (1980). *Linear algebra and its applications*. Academic Press.
- Van Rossum, G., & Drake, F. L. (2009). *Python 3 reference manual*. Scotts Valley, CA: CreateSpace.
- Wohlgemuth, M. (2010). Ein Satz von Carnot. In *Mathematisch für fortgeschrittene Anfänger: Weitere beliebte Beiträge von Matroids Matheplanet* (pp. 273–276). Spektrum Akademischer Verlag.